Heliyon 10 (2024) e33079

Contents lists available at ScienceDirect

Heliyon

journal homepage: www.cell.com/heliyon

Research article

Genomic characteristics of adipose-derived stromal cells induced into neurons based on single-cell RNA sequencing

Xiaodong Yuan [a,b,*,1], Wen Li [a,b,1], Qing Liu [a,b], Qingxi Long [a,b], Qi Yan [a,b], Pingshu Zhang [a,b,**]

[a] Department of Neurology of Kailuan General Hospital Affiliated North China University of Science and Technology, China
[b] Hebei Provincial Key Laboratory of Neurobiological Function, China

ARTICLE INFO

Keywords:
Adipose-derived stromal cells
Induced differentiation response
Neurons
Single-cell RNA sequencing
Gene
Transcription factor

ABSTRACT

Adipose-derived stromal cells (ADSCs) can be induced to differentiate into neurons, representing the most promising avenue for cell therapy. However, the molecular mechanism and genomic characteristics of the differentiation of ADSCs into neurons remain poorly understood. In this study, cells from the adult ADSCs group, induction 1h, 3h, 5h, 6h, and 8h groups were selected for single-cell RNA sequencing (scRNA-Seq). Samples from these seven-time points were sequenced and analyzed. The expression of neuron marker genes, including NES, MAP2, TMEM59L, PTK2B, CHN1, DNM1, NRSN2, FBLN2, SCAMP1, SLC1A1, DLG4, CDK5, and ENO2, was found to be low in the ADSCs group, but highly expressed in differentiated cell clusters. The expression of stem cell marker genes, including CCND1, IL1B, MMP1, MMP3, MYO10, and BMP2, was the highest in the ADSCs cluster. This expression decreased significantly with the extension of induction time. Gene ontology (GO) enrichment analysis of upregulated genes in the induced samples showed that the biological processes related to neuronal differentiation and development, such as neuronal differentiation, projection, and apoptosis, were significantly upregulated with a longer induction time during cell cluster differentiation. The results of the cell communication analysis demonstrated the gradual formation of complex neural network connections between ADSC-derived neurons through receptor and ligand pairs at 5h after the induction of differentiation.

1. Introduction

Neurons, as highly differentiated cells, are irreversibly damaged during neurological disorders, resulting in progressive neuronal degeneration and necrosis [1]. Neurodegenerative diseases such as Alzheimer's disease, Parkinson's disease, and amyotrophic lateral sclerosis lack clinically effective treatments. The most promising treatments are neural regeneration and brain function reconstruction methods such as cell transplantation, which have become a hot spot for current research [2]. However, embryonic cells and bone marrow stromal cells, essential sources of stem cells, are more challenging to research and apply due to their difficulty and expense of

* Corresponding author. Department of Neurology, Kailuan General Hospital affiliated North China University of Science and Technology; addresses: 57 Xinhua East Road, Lubei District, Tangshan City, Hebei Province, 063000, China.
** Corresponding author. Pingshu Zhang. Department of Neurology, Kailuan General Hospital affiliated North China University of Science and Technology; addresses: 57 Xinhua East Road, Lubei District, Tangshan City, Hebei Province, 063000, China.
E-mail addresses: yxd69@sohu.com (X. Yuan), 1977nana@sina.com (P. Zhang).
[1] Xiaodong Yuan and Wen Li are Joint first authors.

https://doi.org/10.1016/j.heliyon.2024.e33079
Received 27 June 2023; Received in revised form 13 June 2024; Accepted 13 June 2024
Available online 14 June 2024

obtaining and the ethical considerations involved [3–5]. In the early 21st century, Zuk et al. isolated adipose-derived stromal cells (ADSCs) from human adipose tissue and demonstrated the ability of ADSCs to differentiate in multiple directions and induce differentiation into a variety of target cells, including osteoblasts, chondrocytes, cardiomyocytes, adipocytes, and neurons [6,7]. Meanwhile, scholars have attracted considerable interest from ADSCs due to their numerous advantages, including a comprehensive source, easy access, low immunogenicity, and fewer ethical issues [8]. A significant body of evidence has demonstrated that ADSC-derived neurons exhibit typical neuronal cellular morphological features, ultrastructure, and electrophysiological functions [1,9]. This provides a theoretical basis for using such neuronal cells to treat degenerative nervous system diseases [2].

During cell-induced differentiation, there is a degree of heterogeneity between cells due to changes in gene expression profiles. However, the genomic changes in these cells are not well characterized. The advent of single-cell RNA sequencing (scRNA-Seq) technology has provided a technical foundation to understand the heterogeneity and genomic changes at the single-cell level [10]. It can detect differential expression in specific cell subpopulations by elucidating gene expression changes during cell differentiation or at different time-courses at single-cell resolution, and cluster expression profiles to infer gene regulatory networks (GRNs) and intercellular communication relationships [11]. In this study, we employed scRNA-Seq technology to sequence cells in the process of the ADSC-induced differentiation into neurons to reveal the genomic changes characterized during the ADSC-induced differentiation response, thus providing a theoretical basis for further improving the efficiency of this induced response and for clinical application.

2. Materials and methods

2.1. Extraction and culture of ADSCs

According to the method of Zhang et al. [12], ADSCs were extracted from the waste adipose tissue obtained by needle aspiration after liposuction of a healthy adult female patient aged 20–35 years in Jinrong Aesthetic Plastic Hospital. Adipose tissue was digested using 0.1 % type I collagenase (Sigma, USA) and incubated for 20 min. The digestion was terminated by the addition of an equal volume of complete DMEM medium (composition: 1 % double-antibody, 15 % fetal bovine serum (FBS) (Gibico, USA), and 84 % high-sugar DMEM (HyClone, USA)). Subsequently, the mixture was then centrifuged at 1000 rpm for 10 min. The upper waste solution was discarded, and the cells were incubated in a complete DMEM medium at 37 °C in a humidified incubator with 5 % CO_2. Subsequently, the medium was changed every 2 days. When the cells covered the bottom of the culture flask, the cells were passaged according to the ratio of 1:2 and continued to be cultured. All experiments on human subjects were conducted in accordance with the Declaration of Helsinki and that all procedures were carried out with the adequate understanding and written consent of the subjects. The study protocol was approved by the Ethics Committee of Kailuan General Hospital.

2.2. Recovery of cryopreserved cells

The ADSCs were stored in a −80 °C refrigerator and rapidly thawed in a 37 °C thermostatic water bath. The action should be as fast as possible (the purpose is to minimize the toxic effect of the freezing solution on the cells), and then the thawed cells will be transferred into a 15 mL centrifuge tube, and 5 mL of culture medium was added and mixed well, and then centrifuged (1000r/min, 5 min). Subsequently, the upper layer of waste liquid was aspirated and discarded, and the lower layer of cell precipitate was retained. 5 mL of fresh medium was added again, gently pipetted and mixed, then transferred to a new medium, labeled, and placed in the incubator. 2 days later, the first medium change was carried out to remove the floating dead cells.

2.3. Preparation of pre-induction solution

The storage bottles containing high glucose DMEM solution, FBS solution, and glass bottles containing β-mercaptoethanol (β-ME) were sterilized under light-proof conditions and placed in the biosafety cabinet under UV light irradiation for 60 min. 10 mL of FBS solution and 3.5 μL of β-ME were injected into sterile 50 mL centrifuge tubes with a sterile pipette, and 40 mL of high glucose DMEM solution was added into centrifuge tubes with a pipette pump. The solution was agitated for 1 min and then filtered through a sterile filter. The solution's final concentration was 1 mmol/L. The solution was sealed with a sealing film and stored at 4 °C under light-proof conditions.

2.4. Preparation of induction solution

The storage bottle with high glucose DMEM solution and the glass bottle with β-ME were sterilized under light-proof conditions and placed in the biosafety cabinet under UV light for 60 min. 17.5 μL of β-ME was injected into a sterile 50 mL centrifuge tube with a sterile pipette, 50 mL of high glucose DMEM solution was injected into the centrifuge tube with a pipette pump, and the solution was blown and mixed for 1 min. The mixture was sterilized by a filter filtered. The final concentration of the miscible liquids is 5 mmol/L. The solution was stored at 4 °C and kept away from light.

2.5. ADSC-induced differentiation reaction experiment and grouping

The 3rd generation of vigorously growing ADSCs was taken, the original stale medium was discarded, and cells were gently rinsed 3 times with preheated saline, and 5 mL of pre-induction solution stored away from light was added dropwise into a culture bottle,

labeled, and continued to culture. After pre-induction for 24h, the cells were pre-induction group. After 24h, the pre-induction solution was discarded, cells were rinsed 3 times again with saline, 5 mL of induction solution was added dropwise, and the cells were formally inducted for 1h, 3h, 5h, 6h, and 8h. The morphological changes of the cells at different time points were observed microscopically, where the 3rd generation ADSCs were used as the uninduced group, the control group.

2.6. Preparation of cell suspensions

The biosafety cabinet was sterilized by applying UV light for 60 min. The trypsin, saline, and complete DMEM culture solution storage bottles were transferred to a 37 °C constant temperature water bath for 60 min to preheat and set aside. The pre-warmed solution storage bottles and culture bottles of ADSCs, inducted pri-1d, 1h, 3h, 5h, 6h, and 8h groups, were placed in the sterilized biosafety cabinet for operation. Firstly, the old complete culture medium was discarded, and the cells were washed gently with saline three times, then 700 μL of trypsin was pipetted into the culture flasks, sealed, and shaken gently, and the flasks were placed under an inverted phase contrast microscope to observe the cell status, and 5 mL of the complete culture medium was added after a large number of cells were suspended in the culture medium and transferred to a 15 mL centrifuge tube.

2.7. Sequencing with the BD Rhapsody system

2.7.1. Sample pretreatment

The prepared single-cell suspension was centrifuged at 300 g for 5 min to remove the cell supernatant, 500 μL of sample buffer (BD Rhapsody) was added, and centrifuged again at 300 g for 5 min to remove the cell supernatant; 500 μL of sample buffer was added, and the cells were resuspended and placed on ice.

2.7.2. Cell counting and activity assays

Cells were resuspended by filtration with a cell sieve to remove cell clumps. Pipette 10 μL of cell suspension from the collection tube and add 10 μL of AO/PI (Acridine Orange/propidium iodide, Countstar), then drop the cell suspension into a cell counting plate and place it on a fluorescent cell counter Countstar (Countstar RigelS2) for 60 s for cell counting and activity assay.

2.7.3. Sequencing

Single cells were captured by randomly distributing a single-cell suspension in 200,000 microwells. Beads with oligonucleotide barcodes were added to saturation so that a bead was paired with a cell in a microwell. A cell-lysis buffer was added so that poly-adenylated RNA molecules could be hybridized with the beads. Beads were collected into a single tube for reverse transcription. During cDNA synthesis, each molecule is tagged with a unique molecular identifier (UMI) [13] at the 5′ end and a cellular barcode to indicate its cellular origin. The BD Rhapsody single-cell whole transcriptome amplification process was applied to prepare the library. The second strand of cDNA was synthesized and then ligated to the WTA junction for universal amplification. PCR amplification of cDNA products. Sequencing libraries were quantified using a high-sensitivity DNA microarray (Agilent) on a Bioanalyzer 2200 and a Qubit high-sensitivity DNA analyzer (Thermo Fisher Science). Each sample library was sequenced by HiSeq XTen (Illumina) at 150bp. Chao Wang, a technician from Shanghai Liebing Biological Company, China, completed the experiments of this sequencing project.

2.8. Sequencing data analysis

2.8.1. Data preprocessing

Using the default parameters of fastp [14]to filter the adapter sequence and remove low-quality reads. Data generated by the BD platform was applied to the UMI tool (v1.0.0) to identify cell barcodes. Raw data were mapped using STAR (v2.5.2b), which has default parameters in the UMI tool standard guide, to obtain UMI counts for each sample. All analyses used the human genome (ensemble hg38, v91) as a reference. We calculated quality control indicators for each cell: percentage of mitochondrial genes and number of total genes expressed. We kept cells with less than 10 % mitochondrial gene expression and more than 200 and less than 10,000 expressed genes. Mitochondrial genes were removed from the gene expression list [15–17].

2.8.2. Data normalization

Import the gene expression matrix results into the R (v3.5.1) statistical environment for further analysis. Data normalization was performed using scran (v1.10.2) in the R package. The nearest neighbor method of the fastMNN function was used to correct batch effects between samples [18,19].

2.8.3. Dimension reduction of scRNA-Seq data

The standardized and batch-corrected data were imported into Seurat (v2.3.4) for downstream analysis and visualization, and the integrated data matrix was subjected to principal component analysis (PCA) [16]. Using the Elbowplot function of Seurat, the top 10 PCs were selected for downstream analysis, and the cells were clustered using unsupervised clustering based on the Graphcluster algorithm with a default resolution setting of 0.8 (res = 0.8) [20]and visualized using t-distributed stochastic neighbor embedding (t-SNE) [21]. Then, cell type identification was performed based on marker genes [22].

2.8.4. Gene enrichment analysis

Gene ontology (GO) was used to annotate the biological processes (BP) of differentially expressed genes (DEGs) with up-regulated expression of each time group during ADSC-induced differentiation to obtain all GOs in which genes were involved. The Fisher test was used to calculate the significance level of each GO (P -Value), thus screening the significant GOs for gene enrichment [23,24].

2.8.5. Branch expression analysis modeling (Beam) analysis

After Monocle simulates the time of differentiation that each cell was at, Beam analysis could show a map of gene expression distribution that gradually increases or decreases with the time of differentiation [16,25].

2.8.6. Transcriptional regulation analysis

The GRNs in cells were analyzed using single-cell regulatory network inference and clustering (SCENIC) to calculate the number of regulated genes and their regulatory strength (AUCellScore) for each transcription factor in the cell and to assess the activity of each regulon (group of transcription factor-binding target genes) in the cell [17]. Through this analysis, we can get the regulation of transcription factors in different cell populations and find the specific transcription factors of each cell Cluster [26].

2.9. Cellular communication analysis

CellPhoneDB (v1.1.0) is a public database of ligands, receptors, and their interactions, which enables systematic analysis of intercellular communication molecules. The membrane, secretory, and peripheral proteins were annotated at different time points [27]. The average value and cellular communication significance were calculated according to the cell matrix obtained by interaction and Seurat standardization.

3. Result

3.1. PCA dimensionality reduction and cell clustering visualization techniques control sample cell quality and data

In this study, the number of cells captured in ADSCs, pri-1d, inducted 1h, 3h, 5h, 6h, and 8h samples were 5325, 7368, 5283, 3324, 4971, 6569, and 6988, respectively, for a total of 39828 cells, and their average Reads per cell assay were 42499, 44358, 38139, 57070, 61298, 37446, and 28353, 61298, 37446, 28353, respectively. The genomic mapping rate of all samples was greater than 90 %, indicating good data quality. The total number of cells after filtering was 38453, and the number of cells in ADSCs, pri-1d, inducted 1h, 3h, 5h, 6h, and 8h samples was 5325, 7091, 5106, 3266, 4843, 6417 and 6405, respectively. Then, scRNA-Seq technology was applied to build a library of transcriptome information of single cells. In this study, based on the Seurat Package, PCA, a commonly used

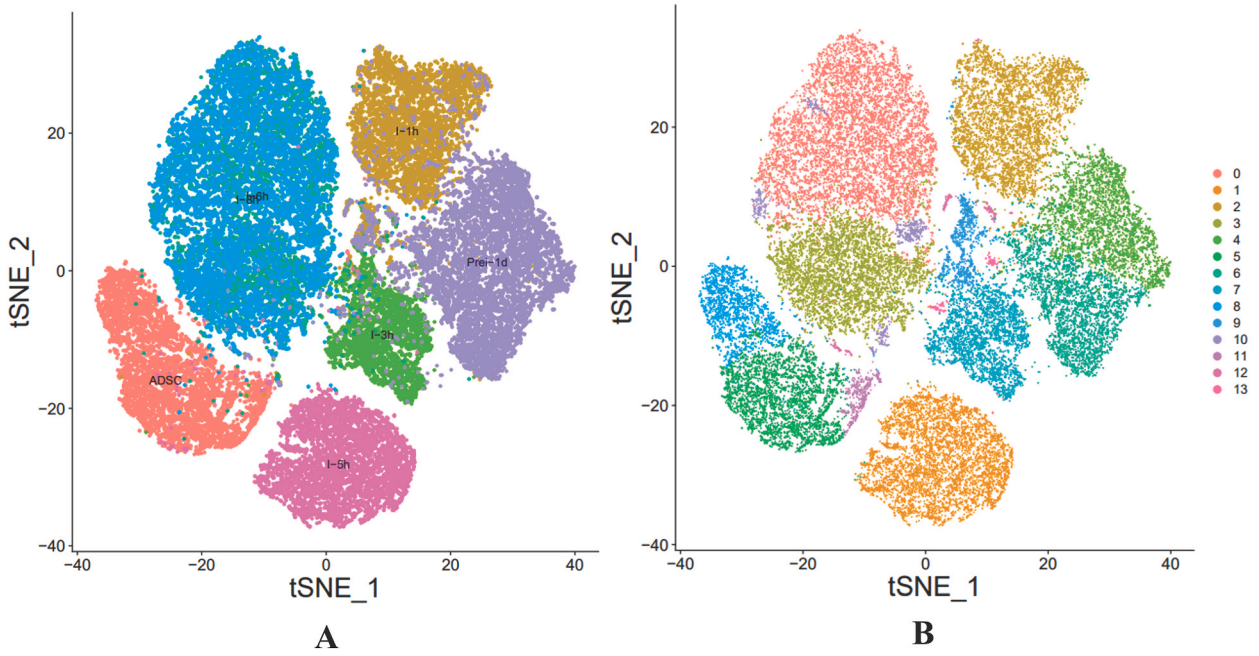

Fig. 1. Results of the 7-time points cell samples with t-SNE visualization presentation.
(A) t-SNE visualization showing the distribution of cells among different samples, with each point in the plot representing a cell and different colors representing different sample sources. (B) The clustering results of all cell t-SNE visualizations, each point represents a cell and the number in the fig. represents the Cluster number of that cell population, divided into 14 Clusters in total.

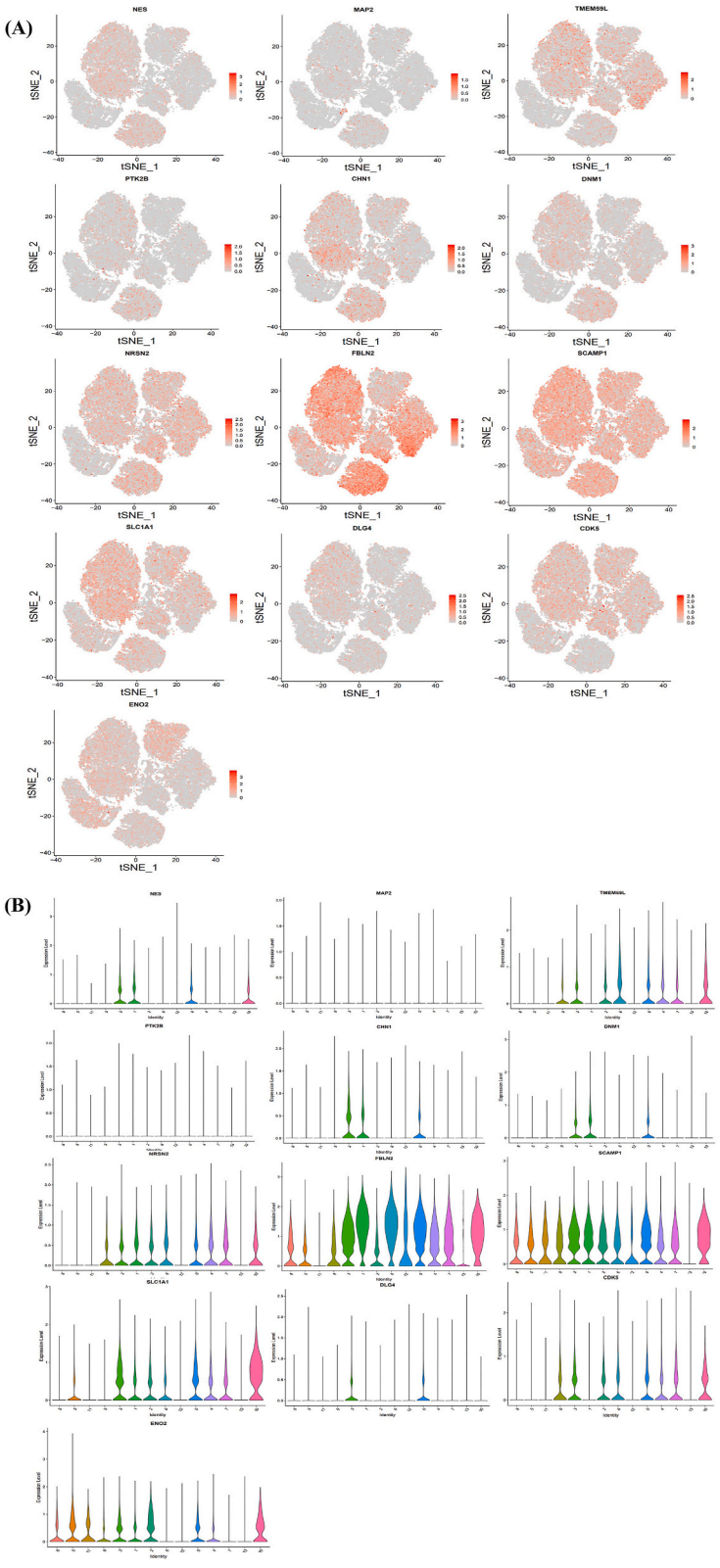

Fig. 2. t-SNE scatter plots and violin plots of the distribution of major neuronal marker genes in each cell cluster.
(A) Scatter plots showing the t-SNE distribution of major neuronal marker genes in each cell cluster. (B) Violin plots showing the distribution of major neuronal marker genes in each cell cluster.

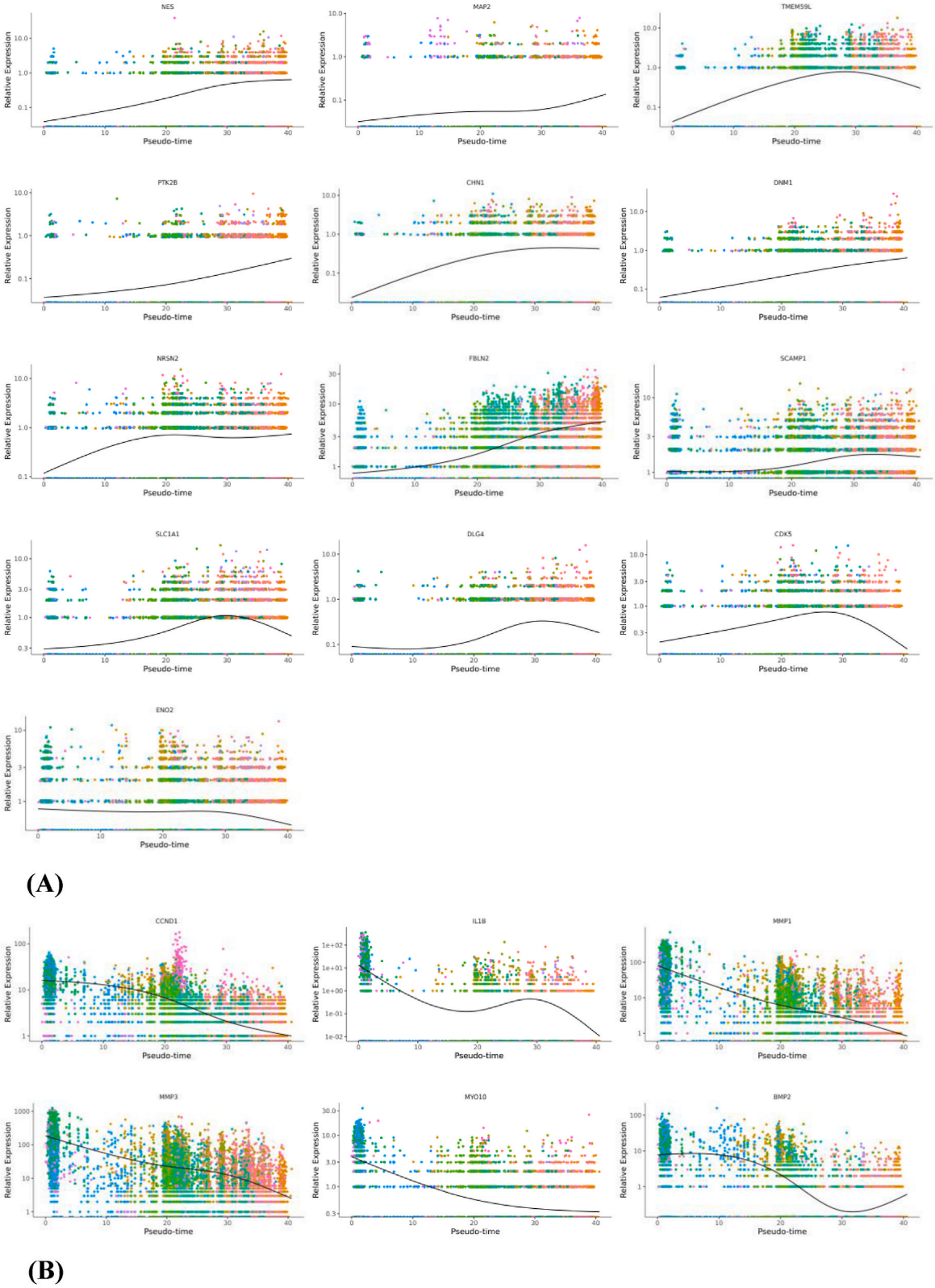

Fig. 3. Beam analysis plots of neuronal and stem cell marker genes.
(A) Beam analysis plots of major neuronal marker genes. (B) Beam analysis plots of the main marker genes of stem cells.

unsupervised linear dimensionality reduction method, was used to reduce the dimensionality of the quality control filtered and normalized data, extract the main features, and the relationship between single cells for t-SNE visualization. Important PCs were selected based on the expression of the most critical gene population occupying the greatest weight in all single-cell samples, and the two principal components (PC1, PC2) that have the most significant impact on individual cells of different samples were localized in a face. The cells of each sample were evenly distributed in each Cluster, and the distance between ADSCs and I-1h was the farthest in the t-SNE plot after inducing them into neurons due to the change of cell type of ADSCs after inducing differentiation (Fig. 1A). All 38453 cells were divided into clusters 0–13 (Fig. 1B), with cells in the ADSCs group mainly distributed in Clusters 5, 8, and 11, cells in the pri-1d group distributed in Clusters 4, 6 and 13, cells in the induction 1h group mainly distributed in Clusters 2, 9 and 12, cells in the induction 3h group were distributed in clusters 7 and 9, the cells in the induction 5h group were mainly distributed in cluster 1. The cells in the induction 6h and 8h groups were mainly distributed in clusters 0, 3, and 10.

3.2. *Pseudo-temporal expression results of major neuronal marker genes in each cell cluster*

The t-SNE distribution scatter plots and violin plots of neuron marker genes NES, MAP2, TMEM59L, PTK2B, CHN1, DNM1, NRSN2, FBLN2, SCAMP1, SLC1A1, DLG4, CDK5, ENO2 were shown in Fig. 2. Fig. 2A is the scatter plots of t-SNE distribution of these neuronal marker genes, and Fig. 2B is the violin plots of the distribution of these neuronal marker genes.

3.3. *Results of Beam analysis of pseudo-time trajectory expression of marker genes in neurons and stem cells*

NES, MAP2, TMEM59L, PTK2B, CHN1, DNM1, NRSN2, FBLN2, SCAMP1, SLC1A1, DLG4, CDK5, ENO2 of neuronal marker genes and CCND1, IL1B, MMP1, MMP3, MYO10, BMP2 of stem cell marker genes of the results of Beam analysis of the expression characteristics along with the pseudo-time trajectory were shown in Fig. 3. With the extension of induction time, the marker genes of neurons gradually showed an upward trend (Fig. 3A), the marker genes of stem cells gradually showed a downward trend (Fig. 3B).

3.4. *Results of up-regulation of BP function in gene-enriched GO of differentiated cells in each group compared to the ADSCs group*

The samples from the pri-1d, induction 1h, 3h, 5h, 6h, and 8h groups were compared with ADSCs, and 1874, 1905, 1958, 2539, 2174, and 2199 differential genes were screened with $P < 0.05$ as the threshold criterion, and 912, 955, 1004, 1164, 1058, and 1066

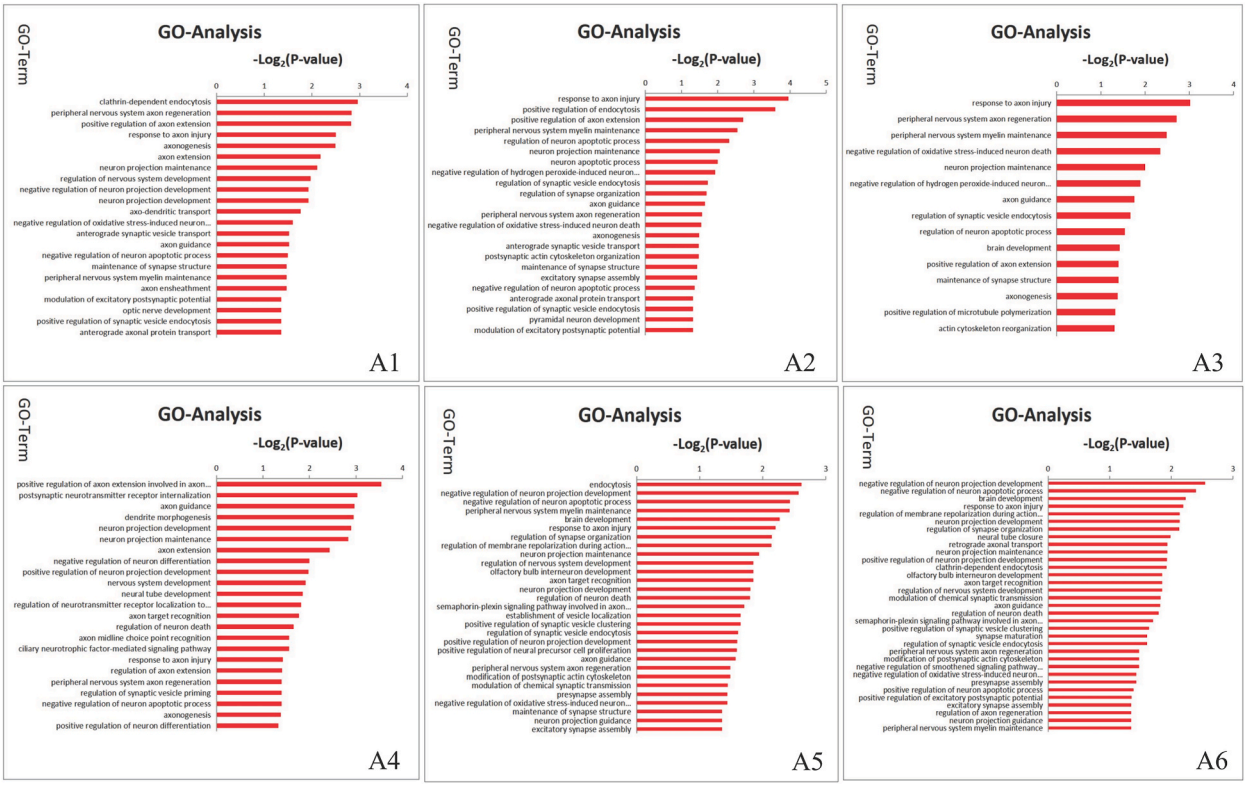

Fig. 4. BP function of up-regulated gene enriched GO for each time point sample compared with ADSCs group. A1-A6 show the BP function of upregulated gene-enriched GO in pri-1d, induction 1h, 3h, 5h, 6h, and 8h groups compared with ADSCs group, respectively (red represents significant entries, $P < 0.05$; blue represents non-significant entries).

differential genes were up-regulated in expression compared with the ADSCs group, respectively. The latter were subjected to BP functional analysis of gene enrichment GO, and the significant entries with $P < 0.05$ associated with neurons were selected and plotted in the tube diagram in Fig. 4. Fig 4A1 shows the BP function of up-regulated gene-enriched GOs in the pri-1d group compared with the ADSC group, and Fig. 4A2-A6 show the BP function of up-regulated gene-enriched GOs in the induced 1h, 3h, 5h, 6h, and 8h groups compared with the ADSC group, respectively.

3.5. Results of activation analysis of gene set expression of cell clusters in each group

Samples at each time point in the heat map presented according to QuSAGE analysis differed in the degree of significant activation in different gene sets. Cluster 0 (induction 6h and 8h) was significant in protein digestion and absorption gene set; cluster 1 (induction 5h) was significant in neuroactive ligand-receptor interaction and fat digestion and absorption gene sets; clusters 2 and 9 (induction 1h and 3h) were significant in synaptic vesicle cycle gene set; and the cluster 3 (induction 6h and 8h) were significant in DNA replication, mismatch repair, and homologous recombination gene sets; the cluster 5 (ADSC) was significant in mineral absorption, IL-17 signaling

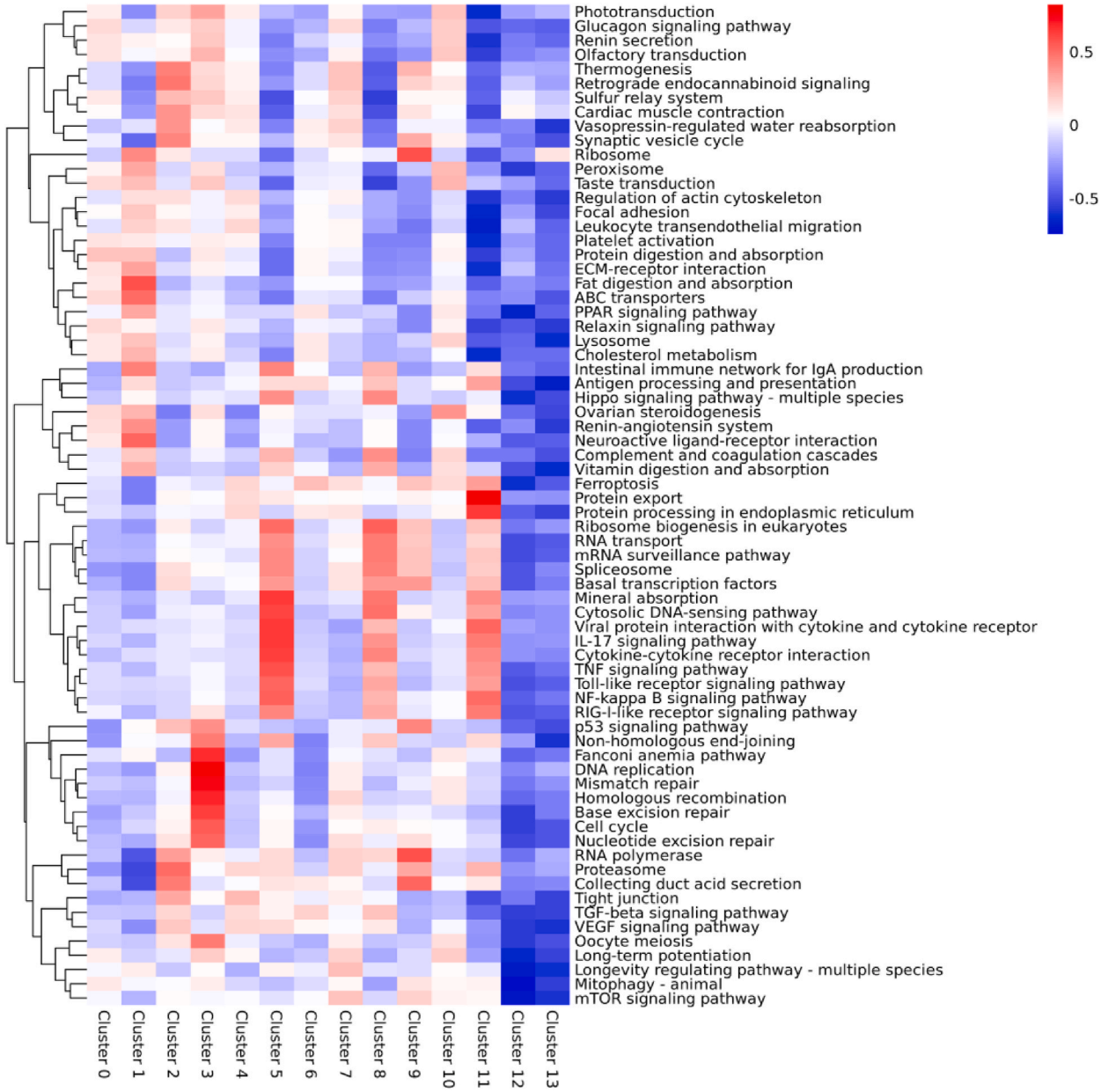

Fig. 5. Heat map of the activation level of different gene sets in each cluster of cells.

pathway, cytokine-cytokine receptor interaction, and TNF signaling pathway gene sets; cluster 8 (ADSC) was in Ribosome biogenesis in eukaryotes, RNA transport gene sets; and cluster 11 (ADSC) was significant in protein export and protein processing in endoplasmic reticulum gene sets (Fig. 5).

3.6. Regulatory intensity of the most strongly expressed transcription factors in each group in each cluster of cells

SCENIC analysis of differential regulation of transcription factors showed that the most strongly regulated transcription factors in each group were JUN in cells of the ADSCs group, MSX1 in cells of the pri-1d and induction 1h groups, DDIT3 in cells of the 3h group, MAFB in cells of the 5h group, and EZH2 in cells of the 6h and 8h groups, respectively (Fig. 6A). In addition, the STAT1 transcription factor had a low regulatory effect in the ADSCs group of cells, but it had a robust regulatory effect in all groups of cells after induction (Fig. 6B).

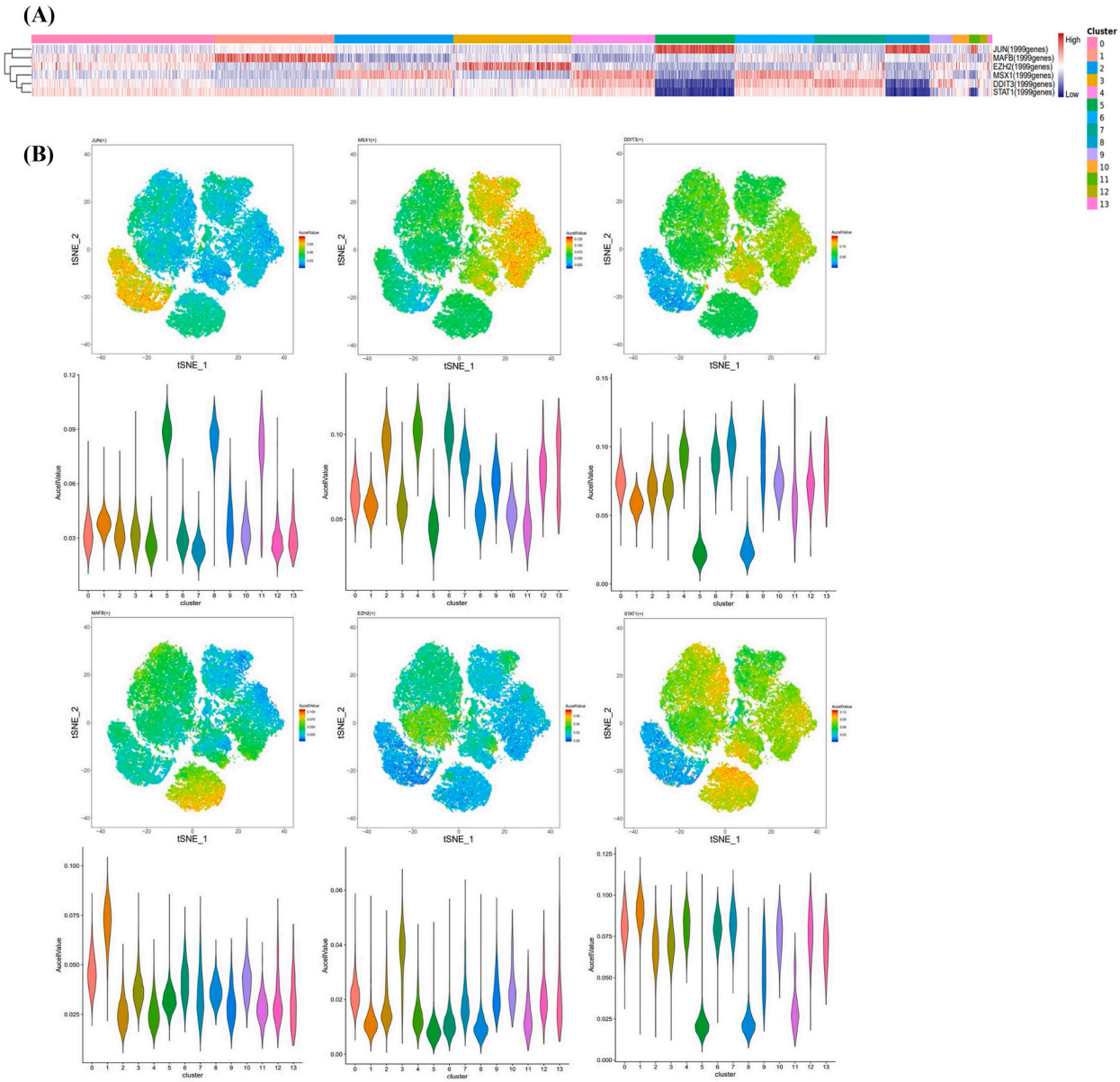

Fig. 6. Regulatory intensity heat plot, t-SNE plots, and violin plots of transcription factors expressed in different samples.
(A) SCENIC analysis reveals the transcription factors with the highest intensity of regulation in each group. (B) t-SNE plots and violin plots of the transcription factors with the highest intensity of regulation in each group.

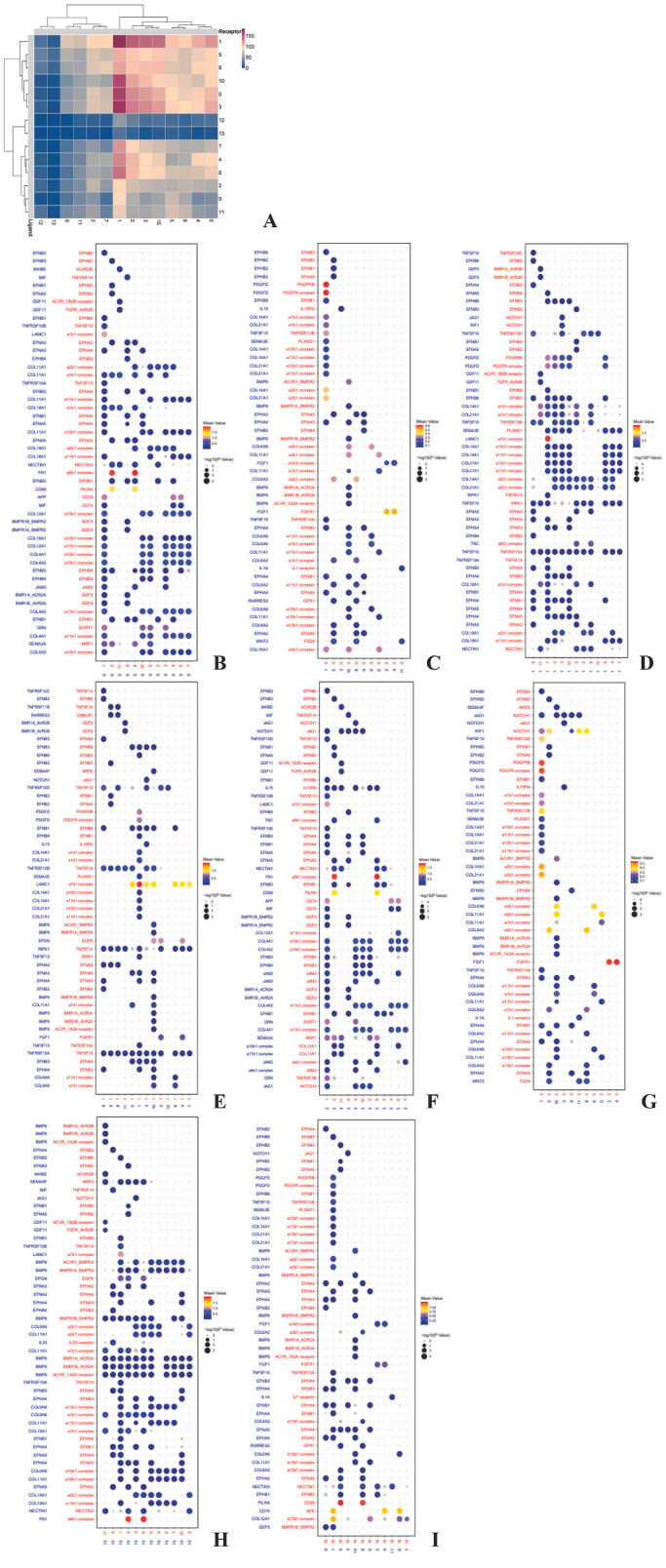

(caption on next page)

Fig. 7. Cell communication results of receptors and ligands between clusters of cells in each group.
(A) Relationship heat map when different clusters are used as ligand and receptor respectively. (B, C) Results of the first 50 relationships in cellular communication with Cluster0 as the rank ascending sequence of ligand and receptor, where the size of the ball represents the p-value and the color shade represents the regulatory strength of the relationship. (D, E) Results of the first 50 relationships in cellular communication with Cluster1 as the rank ascending order of ligand and receptor. (F, G) Results of the first 50 relationships in cellular communication with Cluster 3 as the rank ascending order of ligand and receptor. (H, I) Results of the first 50 relationships in cellular communication with Cluster10 as the rank ascending sequence of ligand and receptor.

3.7. Results of intercellular communication between receptors and ligands for each cluster of cells in each group

CellPhoneDB results of ligand-receptor interactions between cells showed that cluster 1 (5h group) had the most robust ligand-receptor interactions with clusters 1, 0, 3, and 10 (5h, 6h, and 8h groups), followed by stronger ligand interactions with clusters 4, 6, and 7 (pri-1d, 3h groups) for cluster 1. The ligand-receptor interaction was more vital for clusters 0 and 3 (6h and 8h groups). Among them, the FN1 ligand of cluster 0 interacted more strongly with the a8b1 complex receptor of clusters 5 and 8, and the PDGFRB and PDGFR complex receptors of cluster 0 interacted more strongly with the PDGFD ligand of cluster 1 (Fig. 7A). The LAMC1 ligand of cluster 1 interacted more strongly with the a7b1 complex receptor, and the a7b1 complex receptor of cluster 1 interacted more strongly with the LAMC1 ligands of clusters 0, 3, 10, 4, 6, and 7. The FN1 ligand of cluster 3 interacted more strongly with the a8b1 complex receptor of clusters 5 and 8, respectively, the PDGFRB and PDGFR complex receptors of cluster 3 interacted more strongly with the PDGFD ligand of cluster 1, and the FGFR1 receptor of cluster 3 interacted more strongly with the FGF1 ligand of clusters 2 and 4. The FN1 ligand of cluster 10 interacted more strongly with the a8b1 complex receptor of clusters 5 and 8, the CD99 receptor of cluster 10 interacted more strongly with the ligands of clusters 5 and 8, the APP receptor of cluster 10 interacted more strongly with the CD74 ligands of clusters 1, 4 and 6, and the a10b1 complex receptor of cluster 10 interacted more strongly with the COL12A1 ligand of cluster 1 (Fig. 7B–I).

4. Discussion

Our previous studies found that ADSC-induced differentiated neurons have typical neuronal cell morphology, ultrastructure, and neurophysiological functions [1,5,9]. However, the characterization of its genomic changes during this induction response is unclear. We used scRNA-Seq technology to construct a single-cell transcriptome information library, and t-SNE visualization localization was performed to visualize the relationship between ADSCs differentiation into neurons. The t-SNE visualization results at each time point of ADSCs differentiation into neurons were displayed, and these cells were divided into 0–13 clusters. The gene expression characteristics of the cells in each cluster were further analyzed. The neuronal marker genes NES, MAP2, PTK2B, CHN1, DNM1, NRSN2, FBLN2, and SCAMP1 [24,28–34] gradually increased with the induction time, while TMEM59L, SLC1A1, DLG4, CDK5, and ENO2 [35–39] peaked in the induction 5h cell cluster but significantly decreased in the induction 8h cell cluster. However, the expression of CCND1, IL1B, MMP1, MMP3, MYO10, and BMP2 [40–46], stem cell marker genes, were highest in the ADSC cluster and significantly decreased in their differentiated cell clusters with increasing induction time. Meanwhile, the BP functions related to neuronal differentiation and development, such as neuronal differentiation and projection and apoptosis, dendritic morphogenesis, axonogenesis, guidance, extension, protein transport and damage response and regeneration, synaptic assembly, cell transport and regulation of endocytosis in their differentiated cell clusters were significantly up-regulated with longer induction time. The pattern of genomic changes during the induction of differentiation of ADSCs into neurons and the evolutionary characteristics of its cellular functional processes were elucidated. This is crucial to reveal the molecular biological mechanism of its induction of differentiation response.

It has been shown that cells can change from one functional "state" to another during cell growth and development in response to various stimuli [25,47,48]. When cells shift between states, a reorganization of transcription occurs in which some genes are silenced, and others are activated so that the genes are activated and expressed differently in cells in different states [49–52]. Monocle is a classic tool for ScRNA-seq analysis, enabling the study of the sequence of gene expression changes each cell must undergo during cell state transitions. Once the overall "trajectory" of gene expression changes is known, Monocle can place each cell in the appropriate position in the trajectory [53]. After determining the differentiation starting point of ADSCs, Monocle can simulate the differentiation time of each cell, find the heat map and distribution map of gene expression that gradually increases or decreases with the differentiation time, namely Beam analysis, and then obtain the determinant genes related to differentiation [54]. Beam analysis of neuronal marker genes and stem cell marker genes in this study showed the trend of gene expression during the differentiation of ADSCs into neurons. Previous studies have shown that this ADSCs induction response has differentiated into mature neurons by 5h, while continued induction up to 8h results in degenerative aging or even death changes in differentiated cells [1]. This study revealed that CCND1, IL1B, MMP1, MMP3, MYO10, and BMP2, marker genes of stem cells highly expressed in ADSCs, decreased significantly and gradually with increasing induction time. However, the expression of neuronal marker genes such as NES, MAP2, TMEM59L, PTK2B, CHN1, DNM1, NRSN2, FBLN2, SCAMP1, SLC1A1, DLG4, CDK5, ENO2, etc., although low in ADSCs, increased significantly and gradually in differentiated cells as the induction time increased, with MAP2, TMEM59L, SLC1A1, DLG4, CDK5, ENO2 TMEM59L, SLC1A1, DLG4, CDK5, and ENO2 peaked in the cell clusters at 5h of induction but decreased significantly by 8h of induction. This suggests that the latter gene could serve as a marker gene for mature neurons. It also confirms the characteristic of gradual activation of neuron-related genes and gradual silencing of stem cell-related genes in ADSCs during the differentiation of ADSCs into neurons. However, the expression of the proteins corresponding to these genes during the differentiation of ADSCs into neurons is still unclear, which needs to be verified in the next step of the study to provide more options for future studies on selecting neuronal markers.

GO analysis in ScRNA-seq is annotated by calculating whether differential genes in the regulatory process are significantly clustered at three levels: cellular component, molecular function, and biological process [55]. Studies have shown that ADSC-induced differentiation of 5h cells has typical neurons' cytomorphological features and electrophysiological functions of typical neurons [2]. However, only some other functional studies on such ADSC-derived neurons have been reported. Our BP results from this differential gene enrichment GO with neuron-related significant entries of upregulated expression of differentiated cell clusters during the induced differentiation response showed that the functions upregulated in pri-1d were mainly neurite protrusion maintenance and development, axonogenesis and extension, axon-dendritic cell transport, and axon sheath and so on. Upregulated at 1h of induction were mainly the positive regulation of endocytosis, regulation of neuronal apoptotic processes, maintenance and regulation of synaptic structures, organization of the postsynaptic actin cytoskeleton, and neuronal development. Upregulated at induction 3h are mainly positive regulation of microtubule aggregation, actin cytoskeleton reorganization, and negative regulation of oxidative stress-induced neuronal death. The main functions upregulated at induction 5h are involved in axon guidance, postsynaptic neurotransmitter receptor internalization, dendrite morphogenesis, negative regulation of neuron differentiation, nervous system development, neural tube development, regulation of neurotransmitter receptor localization to postsynaptic specialization membrane, axon target recognition, axon midline choice point recognition, ciliary neurotrophic factor-mediated signaling pathway, regulation of axon extension, regulation of synaptic vesicle priming, positive regulation of neuron differentiation. Upregulated at 6h of induction is mainly the establishment of vesicle localization, the regulation of membrane repolarization during action potentials, the modification of the postsynaptic actin cytoskeleton, and the regulation of chemical synaptic transmission. The main functions upregulated at induction 8h are the positive regulation of synaptic vesicle aggregation, synaptic maturation, synaptic vesicle endocytosis, and positive regulation of excitatory postsynaptic potentials. This suggests that differentiated cells at different times during this induction differentiation reaction have different functions associated with neurons and that differentiated cells at 5h of induction already have the structure and function of neurons. Therefore, termination induction response can be performed on 5h cells in the following studies to obtain cells for functional verification and provide a new source for cell transplantation therapy.

The basis of cell heterogeneity is the difference in cell transcription state, and the heterogeneity of transcription state is determined and maintained by GNRs dominated by transcription factors [56]. Therefore, the analysis of GRNs in single cells can help to explore the biological significance behind cellular heterogeneity and provide valuable clues for the study of disease diagnosis, treatment, and developmental differentiation. SCENIC is an algorithm for GRNs developed specifically for single-cell data that identifies highly reliable GRNs dominated by transcription factors by inferring gene co-expression networks [57]. To analyze the GRNs during ADSC-induced differentiation into neurons, the results of our SCENIC study showed different transcription factors with the highest specific expression at different time points, suggesting a large variability in the regulation of transcription factors between samples at each time point. The most strongly regulated transcription factor in ADSCs was JUN, while in differentiated cells at 1h of induction of differentiation, the reaction was MSXI, at 3h was DDIT3, at 5h was MAFB, and at 6h and 8h was EZH2. Meanwhile, although STAT1 had a low regulatory role in ADSCs, the regulatory role increased significantly and gradually with the prolongation of the induction response time. This indicates that different transcription factors regulate cells during the induction differentiation response at different times. JUN is a crucial transcription factor for maintaining the function of ADSCs. In contrast, MSXI, DDIT3, MAFB, EZH2, STAT1, and other transcription factors play critical regulatory roles during this induction differentiation response, resulting in differentiated cells with different cell morphology and functions at different times.

In addition, cell communication studies based on the CellPhoneDB database have revealed that specific ligand-receptor interactions occur between clusters of cells during this induced differentiation response. The results showed the most robust ligand-receptor interaction between the 1 cluster of cells at induction 5h and the 1, 0, 3, and 10 clusters of cells at induction 5h, 6h, and 8h, with the most substantial communication-linkage effect between cells within the induction 5h group, followed by the ligand-receptor interaction between the 5h group and the cells at induction 6h and 8h, and the ligand-receptor interaction between the cells at induction 6h and 8h.This was followed by a more vital receptor interaction of the 1-cluster ligand with the 4, 6, and 7 clusters of cells that are pri-1d and induction 3h. This is mainly reflected by the strong interaction between LAMC1 ligands of cluster 1 and a7b1 complex receptors, the strong interaction between PDGFD ligands of cluster 1 and PDGFRB and PDGFR complex receptors of cluster 0, and the strong interaction between a7b1 complex receptors of cluster 1 and LAMC1 ligands of clusters 0, 3, 10, 4, 6, and 7. The PDGFD ligand of cluster 1 interacts more strongly with the PDGFRB and PDGFR complex receptors of cluster 3. The COL12A1 ligand of cluster 1 interacts more strongly with a10b1 complex receptors of cluster 10. However, this cellular communication link between pri-1d, induction 1h, and 3h differentiated cells was weak. The results of the cell cluster gene set expression activation analysis in this study also confirmed the significant activation of the neuroactive ligand−receptor interaction gene set between cluster 1 of cells at induction 5h. The results indicate that this complex neural network pathway of interconnection between ADSC-derived mature neurons is gradually formed through receptor-ligand pairs. This neural network pathway is formed mainly in the form of cellular communication links between cellular ligands and receptors starting at 5h of the induction of the differentiation response. Also, the interaction of this mode of communication between the clusters of cells plays a vital role in this induced differentiation response. However, the above analysis results need to be further verified to reveal the diversity and complexity of ADSC-derived neurons further and provide a new direction for cell research and treatment in the future.

5. Conclusion

In summary, scRNA-Seq was applied to discover the genomic changes in ADSC-induced differentiation into neurons, revealing that this complex neural network of interconnections between ADSC-derived neurons through receptor-ligand pairs is gradually formed mainly from 5h of the induction response, which provides a theoretical basis to clarify the molecular biological mechanism of this

induction response.

Ethics declarations

This study was reviewed and approved by the Ethics Committee of Kailuan General Hospital in Tangshan, Hebei Province, China. with the approval number: [2018010]. All patients (or their proxies/legal guardians) provided informed consent to participate in the study.

Funding statement

This work was supported by the 2020 Hebei Provincial Innovation Capacity Improvement Program–Special Project for the Construction of Science and Technology R&D Platforms and New R&D Institutions (grant number:20567622H), Tangshan Science and Technology Research and Development Project in 2020(grant number: 20130210D).

Data availability statement

Data will be made available on request.

CRediT authorship contribution statement

Xiaodong Yuan: Writing – review & editing, Supervision, Methodology, Data curation. **Wen Li:** Visualization, Investigation. **Qing Liu:** Writing – original draft, Validation, Formal analysis. **Qingxi Long:** Visualization, Investigation. **Qi Yan:** Visualization, Investigation. **Pingshu Zhang:** Writing – original draft, Validation, Formal analysis.

Declaration of competing interest

The authors declare that they have no known competing financial interests or personal relationships that could have appeared to influence the work reported in this paper.

Acknowledgments

Thank you to Tangshan Jinrong Beauty Hospital for contributing to the adipose tissue specimens utilized in this study. Thanks to Wu Xiaoying, Zhang Jian, Tao Li, and other Hebei Neurobiological Function Key Laboratory professors for their assistance with the experiment.

References

[1] Y. Lu, et al., Autophagy and apoptosis during adult adipose-derived stromal cells differentiation into neuron-like cells in vitro, Neural Regen Res 7 (16) (2012) 1205–1212, https://doi.org/10.3969/j.issn.1673-5374.2012.16.001.
[2] Y. Lu, et al., Autophagy activator promotes neuronal differentiation of adult adipose-derived stromal cells, Neural Regen Res 8 (10) (2013) 882–889, https://doi.org/10.3969/j.issn.1673-5374.2013.10.002.
[3] Y. Ou, et al., Ultrastructure and electrophysiology of astrocytes differentiated from adult adipose-derived stromal cells, Chin Med J (Engl). 124 (17) (2011) 2656–2660. https://www.ncbi.nlm.nih.gov/pubmed/22040419.
[4] Q. Sun, et al., The effect of autophagy in the process of adipose-derived stromal cells differentiation into astrocytes, J. Mol. Neurosci. 53 (4) (2014) 608–616, https://doi.org/10.1007/s12031-014-0227-5.
[5] Q. Wang, et al., The relationship between the Bcl-2/Bax proteins and the mitochondria-mediated apoptosis pathway in the differentiation of adipose-derived stromal cells into neurons, PLoS One 11 (10) (2016) e0163327, https://doi.org/10.1371/journal.pone.0163327.
[6] P.A. Zuk, et al., Multilineage cells from human adipose tissue: implications for cell-based therapies, Tissue Eng. 7 (2) (2001) 211–228, https://doi.org/10.1089/107632701300062859.
[7] P.A. Zuk, et al., Human adipose tissue is a source of multipotent stem cells, Mol. Biol. Cell 13 (12) (2002) 4279–4295, https://doi.org/10.1091/mbc.e02-02-0105.
[8] X. Yuan, et al., Mitochondrial apoptosis and autophagy in the process of adipose-derived stromal cell differentiation into astrocytes, Cell Biol. Int. 40 (2) (2016) 156–165, https://doi.org/10.1002/cbin.10548.
[9] X. Yuan, et al., Adult adipose-derived stromal cells differentiate into neurons with normal electrophysiological functions, Neural Regen Res 6 (34) (2011) 2681–2686, https://doi.org/10.3969/j.issn.1673-5374.2011.34.006.
[10] T.K. Olsen, , et al.N. Baryawno, Introduction to single-cell RNA sequencing, Curr. Protoc. Mol. Biol. 122 (1) (2018) e57, https://doi.org/10.1002/cpmb.57.
[11] C. Cheng, et al., A review of single-cell RNA-seq annotation, integration, and cell-cell communication, Cells 12 (15) (2023) 1970, https://doi.org/10.3390/cells12151970.
[12] L. Zhang, et al., The relationship between mitochondrial fusion/fission and apoptosis in the process of adipose-derived stromal cells differentiation into astrocytes, Neurosci. Lett. 575 (2014) 19–24, https://doi.org/10.1016/j.neulet.2014.05.025.
[13] T. Smith, et al., UMI-tools: modeling sequencing errors in Unique Molecular Identifiers to improve quantification accuracy, Genome Res. 27 (3) (2017) 491–499, https://doi.org/10.1101/gr.209601.116.
[14] S. Chen, et al., fastp: an ultra-fast all-in-one FASTQ preprocessor, Bioinformatics 34 (17) (2018) i884–i890, https://doi.org/10.1093/bioinformatics/bty560.
[15] Q. Liu, et al., Investigate the stemness of adult adipose-derived stromal cells based on single-cell RNA-sequencing, Cell Biol. Int. 46 (12) (2022) 2118–2131, https://doi.org/10.1002/cbin.11898.
[16] F. Wu, et al., Single cell transcriptomics reveals lineage trajectory of retinal ganglion cells in wild-type and Atoh7-null retinas, Nat. Commun. 12 (1) (2021) 1465, https://doi.org/10.1038/s41467-021-21704-4.

[17] M. Li, et al., Single-cell regulatory network inference and clustering identifies cell-type specific expression pattern of transcription factors in mouse sciatic nerve, Front. Cell. Neurosci. 15 (2021) 676515, https://doi.org/10.3389/fncel.2021.676515.
[18] Z. Chen, et al., Single-cell RNA sequencing highlights the role of inflammatory cancer-associated fibroblasts in bladder urothelial carcinoma, Nat. Commun. 11 (1) (2020) 5077, https://doi.org/10.1038/s41467-020-18916-5.
[19] S. Gao, Data analysis in single-cell transcriptome sequencing, Methods Mol. Biol. 1754 (2018) 311–326, https://doi.org/10.1007/978-1-4939-7717-8_18.
[20] R. Zhang, et al., Cell populations in neonatal rat peripheral nerves identified by single-cell transcriptomics, Glia 69 (3) (2021) 765–778, https://doi.org/10.1002/glia.23928.
[21] D. Kobak, , et al.P. Berens, The art of using t-SNE for single-cell transcriptomics, Nat. Commun. 10 (1) (2019) 5416, https://doi.org/10.1038/s41467-019-13056-x.
[22] H. Sun, et al., Single-cell RNA-seq analysis identifies meniscus progenitors and reveals the progression of meniscus degeneration, Ann. Rheum. Dis. 79 (3) (2020) 408–417, https://doi.org/10.1136/annrheumdis-2019-215926.
[23] M. Ashburner, et al., Gene ontology: tool for the unification of biology. The Gene Ontology Consortium, Nat. Genet. 25 (1) (2000) 25–29, https://doi.org/10.1038/75556.
[24] S. Zhong, et al., A single-cell RNA-seq survey of the developmental landscape of the human prefrontal cortex, Nature 555 (7697) (2018) 524–528, https://doi.org/10.1038/nature25980.
[25] J. Wang, et al., Quick commitment and efficient reprogramming route of direct induction of retinal ganglion cell-like neurons, Stem Cell Rep. 15 (5) (2020) 1095–1110, https://doi.org/10.1016/j.stemcr.2020.09.008.
[26] S. Aibar, et al., SCENIC: single-cell regulatory network inference and clustering, Nat. Methods 14 (11) (2017) 1083–1086, https://doi.org/10.1038/nmeth.4463.
[27] M. Efremova, et al., CellPhoneDB: inferring cell-cell communication from combined expression of multi-subunit ligand-receptor complexes, Nat. Protoc. 15 (4) (2020) 1484–1506, https://doi.org/10.1038/s41596-020-0292-x.
[28] E.-R. Consortium, et al., De novo mutations in synaptic transmission genes including DNM1 cause epileptic encephalopathies, Am. J. Hum. Genet. 95 (4) (2014) 360–370, https://doi.org/10.1016/j.ajhg.2014.08.013.
[29] C. Angelini, et al., CHN1 and duane retraction syndrome: expanding the phenotype to cranial nerves development disease, Eur. J. Med. Genet. 64 (4) (2021) 104–188, https://doi.org/10.1016/j.ejmg.2021.104188.
[30] L. Dehmelt, , et al.S. Halpain, The MAP2/Tau family of microtubule-associated proteins, Genome Biol. 6 (1) (2005) 204, https://doi.org/10.1186/gb-2004-6-1-204.
[31] L. Fagerberg, et al., Analysis of the human tissue-specific expression by genome-wide integration of transcriptomics and antibody-based proteomics, Mol. Cell. Proteomics 13 (2) (2014) 397–406, https://doi.org/10.1074/mcp.M113.035600.
[32] K.M. Hao, et al., [Time dependent expression profiling of PTK2B and its relationship with Aβ, Tau and LRP-1 in hippocampus and blood of APPswe/PS1dE9 double-transgenic mouse, Zhongguo Ying Yong Sheng Li Xue Za Zhi 38 (1) (2022) 17–24, https://doi.org/10.10247/j.cjap.6191.2022.004.
[33] Z. Khosravizadeh, et al., The beneficial effect of encapsulated human adipose-derived stem cells in alginate hydrogel on neural differentiation, J. Biomed. Mater. Res. B Appl. Biomater. 102 (4) (2014) 749–755, https://doi.org/10.1002/jbm.b.33055.
[34] J. Zhang, , et al.D. Castle, Regulation of fusion pore closure and compound exocytosis in neuroendocrine PC12 cells by SCAMP1, Traffic 12 (5) (2011) 600–614, https://doi.org/10.1111/j.1600-0854.2011.01170.x.
[35] C. Ao, et al., The role of Cdk5 in neurological disorders, Front. Cell. Neurosci. 16 (2022) 951, https://doi.org/10.3389/fncel.2022.951202, 202.
[36] A. Rodríguez-Palmero, et al., DLG4-related synaptopathy: a new rare brain disorder, Genet. Med. 23 (5) (2021) 888–899, https://doi.org/10.1038/s41436-020-01075-9.
[37] L. Tagliafierro, et al., Gene expression analysis of neurons and astrocytes isolated by laser capture microdissection from frozen human brain tissues, Front. Mol. Neurosci. 9 (2016) 72, https://doi.org/10.3389/fnmol.2016.00072.
[38] I. Tirosh, et al., Single-cell RNA-seq supports a developmental hierarchy in human oligodendroglioma, Nature 539 (7628) (2016) 309–313, https://doi.org/10.1038/nature20123.
[39] Q. Zheng, et al., The neuron-specific protein TMEM59L mediates oxidative stress-induced cell death, Mol. Neurobiol. 54 (6) (2017) 4189–4200, https://doi.org/10.1007/s12035-016-9997-9.
[40] S.Y. Park, et al., Ex vivo bone morphogenetic protein 2 gene delivery using periodontal ligament stem cells for enhanced re-osseointegration in the regenerative treatment of peri-implantitis, J. Biomed. Mater. Res. 103 (1) (2015) 38–47, https://doi.org/10.1002/jbm.a.35145.
[41] A.N. Raines, et al., Headless Myo10 is a negative regulator of full-length Myo10 and inhibits axon outgrowth in cortical neurons, J. Biol. Chem. 287 (30) (2012) 24873–24883, https://doi.org/10.1074/jbc.M112.369173.
[42] K. Kessenbrock, et al., A role for matrix metalloproteinases in regulating mammary stem cell function via the Wnt signaling pathway, Cell Stem Cell 13 (3) (2013) 300–313, https://doi.org/10.1016/j.stem.2013.06.005.
[43] H.J. Lee, et al., Tonsil-derived mesenchymal stem cells enhance allogeneic bone marrow engraftment via collagen IV degradation, Stem Cell Res. Ther. 12 (1) (2021) 329, https://doi.org/10.1186/s13287-021-02414-6.
[44] S. Zhu, et al., The miR-145-MMP1 axis is a critical regulator for imiquimod-induced cancer stemness and chemoresistance, Pharmacol. Res. 179 (2022) 106196, https://doi.org/10.1016/j.phrs.2022.106196.
[45] C.A. Mitchell, et al., Stromal niche inflammation mediated by IL-1 signalling is a targetable driver of haematopoietic ageing, Nat. Cell Biol. 25 (1) (2023) 30–41, https://doi.org/10.1038/s41556-022-01053-0.
[46] X. Zhang, et al., YTHDF3 modulates hematopoietic stem cells by recognizing RNA m(6)A modification on Ccnd1, Haematologica 107 (10) (2022) 2381–2394, https://doi.org/10.3324/haematol.2021.279739.
[47] H. Li, et al., Attenuation of PRRX2 and HEY2 enables efficient conversion of adult human skin fibroblasts to neurons, Biochem. Biophys. Res. Commun. 516 (3) (2019) 765–769, https://doi.org/10.1016/j.bbrc.2019.06.089.
[48] S. Mukherjee, et al., Molecular estimation of neurodegeneration pseudotime in older brains, Nat. Commun. 11 (1) (2020) 5781, https://doi.org/10.1038/s41467-020-19622-y.
[49] T.R. Hammond, et al., Single-cell RNA sequencing of microglia throughout the mouse lifespan and in the injured brain reveals complex cell-state changes, Immunity 50 (1) (2019) 253–271.e256, https://doi.org/10.1016/j.immuni.2018.11.004.
[50] R. Hernández, et al., Differentiation of human mesenchymal stem cells towards neuronal lineage: clinical trials in nervous system disorders, Biomol Ther (Seoul). 28 (1) (2020) 34–44, https://doi.org/10.4062/biomolther.2019.065.
[51] P.W. Hook, et al., Single-cell RNA-seq of mouse dopaminergic neurons informs candidate gene selection for sporadic Parkinson disease, Am. J. Hum. Genet. 102 (3) (2018) 427–446, https://doi.org/10.1016/j.ajhg.2018.02.001.
[52] J.S. Toma, et al., Peripheral nerve single-cell analysis identifies mesenchymal ligands that promote axonal growth, eneuro 7 (3) (2020), https://doi.org/10.1523/eneuro.0066-20.2020.
[53] K. Jean-Baptiste, et al., Dynamics of gene expression in single root cells of Arabidopsis thaliana, Plant Cell 31 (5) (2019) 993–1011, https://doi.org/10.1105/tpc.18.00785.
[54] H. Wang, , et al.L. Dou, Single-cell RNA sequencing reveals hub genes of myocardial infarction-associated endothelial cells, BMC Cardiovasc. Disord. 24 (1) (2024) 70, https://doi.org/10.1186/s12872-024-03727-z.

[55] Y. Jiang, et al., Identification of a six-gene prognostic signature for bladder cancer associated macrophage, Front. Immunol. 13 (2022) 930352, https://doi.org/10.3389/fimmu.2022.930352.
[56] C.D. Arcuschin, et al., Mechanisms of robustness in gene regulatory networks involved in neural development, Front. Mol. Neurosci. 16 (2023) 1114015, https://doi.org/10.3389/fnmol.2023.1114015.
[57] C. Bravo González-Blas, et al., SCENIC+: single-cell multiomic inference of enhancers and gene regulatory networks, Nat. Methods 20 (9) (2023) 1355–1367, https://doi.org/10.1038/s41592-023-01938-4.